metals

MDPI

Article

A New Atomistic Mechanism for Heterogeneous Nucleation in the Systems with Negative Lattice Misfit: Creating a 2D Template for Crystal Growth

Zhongyun Fan *, Hua Men, Yun Wang and Zhongping Que

BCAST, Brunel University London, Uxbridge, Middlesex UB8 3PH, UK; hua.men@brunel.ac.uk (H.M.); yun.wang@brunel.ac.uk (Y.W.); zhongping.que@brunel.ac.uk (Z.Q.)
* Correspondence: zhongyun.fan@brunel.ac.uk

Abstract: Heterogeneous nucleation is a widespread phenomenon in both nature and technology. However, our current understanding is largely confined to the classical nucleation theory (CNT) postulated over a century ago, in which heterogeneous nucleation occurs stochastically to form a spherical cap facilitated by a substrate. In this paper, we show that heterogeneous nucleation in systems with negative lattice misfit completes deterministically within three atomic layers by structural templating to form a two-dimentional template from which the new phase can grow. Using molecular dynamics (MD) simulations of a generic system containing metallic liquid (Al) and a substrate of variable lattice misfit (fcc lattice with fixed Al atoms), we found that heterogeneous nucleation proceeds layer-by-layer: the first layer accommodates misfit through a partial edge dislocation network; the second layer twists an angle through a partial screw dislocation network to reduce lattice distortion; and the third layer creates a crystal plane of the solid (the 2D nucleus) that templates further growth. The twist angle of the solid relative to the substrate as a signature of heterogeneous nucleation in the systems with negative lattice misfit has been validated by high resolution transmission electron microscopic (HRTEM) examination of TiB_2/Al and TiB_2/α-$Al_{15}(Fe,Mn)_3Si_2$ interfaces in two different Al-alloys.

Keywords: heterogeneous nucleation; MD simulation; solidification; interface

Citation: Fan, Z.; Men, H.; Wang, Y.; Que, Z. A New Atomistic Mechanism for Heterogeneous Nucleation in the Systems with Negative Lattice Misfit: Creating a 2D Template for Crystal Growth. *Metals* **2021**, *11*, 478. https://doi.org/10.3390/met11030478

Academic Editor: Ayrat Nazarov

Received: 9 February 2021
Accepted: 10 March 2021
Published: 13 March 2021

1. Introduction

Nucleation of crystals in liquids is one of the most ubiquitous phenomena in both natural and industrial processes [1,2]. Understanding nucleation is of vital importance to both science and technology, such as ice nucleation for climate change [3,4], solidification and casting of advanced metallic materials [5], manipulation of nucleation of molecular crystals in the context of drug design and production [6] and protein crystal formation in living beings [7]. However, our current understanding of nucleation is far from complete; and nucleation research has been dominated by the classical nucleation theory (CNT) for more than a century. Theoretically, there is a massive gap of 10^{10}·m^{-3}s^{-1} in the homogeneous ice nucleation rate between CNT-based computer simulations and experimental measurements that has triggered an intense debate between theoreticians and experimentalists [4]. Practically, the CNT provides little guidance to nucleation control in important industrial processes. For example, although the TiB_2 based grain refiner has been used in metallurgical industry for over 70 years [8], it was mainly developed by trial-and-error with little help from the CNT.

The CNT was postulated over a century ago. Based on Gibb's ideas of nucleation [9], the first complete theory of homogeneous nucleation was formulated by Volmer and Weber [10], which was improved by Becker and Döring [11], completed by Zeldovich [12] and extended later to heterogeneous nucleation (see reviews in references [1,2,13]). In the classical homogeneous nucleation theory, a nucleus is formed through structural fluctuation

and the solid/liquid interface is created as a by-product [1]. The CNT applies continuum thermodynamics to determine the critical nucleus size and the energy barrier for its formation and utilizes statistical mechanics to formulate the nucleation rate that describes the nucleation kinetics [10–12]. In the case of heterogeneous nucleation, a substrate facilitates nucleation by reducing the energy barrier. Core to the CNT is its capillarity assumption (thermodynamics) and its fluctuation mechanism for nucleus creation (kinetics). Such assumptions encompass most of the strength and weaknesses of the theory [4]. CNT is conceptually simple, mathematically rigorous, and widely applicable to qualitatively describe many phase transformations and has dominated our thinking for more than a century. However, it does not always relate well to reality, and so far, it has very rarely (if at all) demonstrated homogeneous nucleation by experiments [1].

In recent years, there has been a renaissance of nucleation research [4,14,15], which was initiated from ice nucleation for climate change [3,4] and facilitated by the significant advances in analytical instruments (such as electron microscopy [16], synchrotron imaging [17]) and increased capability for computer simulations [18]. Major advances include, for example, adsorption at the liquid/substrate interface [13], the discovery of stable prenucleation clusters (PNCs) in aqueous solutions [19], the two-step nucleation pathway [20], barrier-less nucleation of 1D crystals [21] and observation of nucleation in 4D [17].

Study of atomic ordering in the liquid adjacent to a liquid/substrate interface has been a hot topic in recent years [22]. Real-time observations with high resolution transmission electron microscopy (HRTEM) showed that liquid aluminum has distinct layering with six atomic peaks [23] and in-plane atomic ordering within the first three atomic layers adjacent to the (0001) α-Al_2O_3 substrate [24]. Computer simulations also revealed that the pronounced atomic ordering persists in the liquid at the liquid/substrate interface even at temperatures above the liquidus [25–27]. More recently, our MD simulations have confirmed the existence of a 2D ordered structure at the liquid/substrate interface, which is referred to as prenucleation [28]. It was reported that a "prefreezing" layer of crystalline Pb, approximately 2–3 atomic layers in thickness, formed at the interface between liquid Pb and (111) Cu substrate at 625 K [29]. Further atomistic simulations have found that prenucleation is strongly dependent on temperature [28,30], lattice misfit between the substrate and the solid derived from the liquid upon solidification [28], chemical interaction between the substrate and the liquid [30] and atomic level surface roughness of the substrate [31]. In addition, recent *in situ* observations with synchrotron X-ray scattering techniques have confirmed that the nucleation potency of a crystalline substrate is highly dependent on the lattice misfit [32].

Prenucleation may either facilitate or impede heterogeneous nucleation depending on the compatibility between the 2D structure created by prenucleation and the new solid phase. For instance, the formation of a (112) Al_3Ti 2D compound (2DC) on the (0001) TiB_2 surface makes TiB_2 particles extremely potent for heterogeneous nucleation of α-Al [16]; while the pentagonal Au layer on the (111) Si substrate has a quasicrystal structure that acts as a main barrier for heterogeneous nucleation in AuSi eutectic droplets [33]. Using *ab initio* MD simulations, Wang et al. [34] observed that an fcc-like atomic ordering exists within three atomic layers in liquid Al at the interface with Ti-terminated (0001) TiB_2 substrate at a small undercooling of around 2 K, and that further growth of the α-Al is frustrated by the lattice misfit between solid Al and TiB_2 substrate.

Recently, we have investigated the atomistic mechanisms of heterogeneous nucleation in metallic liquid/substrate systems with positive lattice misfit (i.e., the solid has larger atomic spacing than the substrate) using MD simulations [35]. We found that building on the 2D ordered structure (the precursor) created by prenucleation, heterogeneous nucleation proceeds layer-by-layer and completes within three atomic layers to create a crystal plane of the solid phase, which act as a 2D nucleus to template further growth. During the nucleation process, the first layer is epitaxial to the substrate surface and is mainly formed at the prenucleation stage; the second layer accommodates all the lattice

misfit by formation of vacancies; and the third layer becomes a plane of the solid (the 2D nucleus) that completes nucleation and starts to template further growth. This has been named as a three-layer nucleation mechanism [35].

In this paper, we studied the heterogeneous nucleation process in generic metallic liquid/substrate systems with negative lattice misfit (i.e., the solid has smaller atomic spacing than the substrate) using classical molecular dynamics (MD) simulations. Based on the simulation results we have established an atomistic mechanism for heterogeneous nucleation in systems with negative misfit, and the key features of the proposed mechanism will be validated by experiments.

2. Simulation and Experimental Methods

2.1. Simulation Approaches

A generic metallic simulation system was created to simulate heterogeneous nucleation process to ensure wider applicability beyond specific systems. It is now well accepted that heterogeneous nucleation is affected by lattice misfit between the solid and the substrate (structural effect) [28], chemical interaction between the liquid and substrate (chemical effect) [30], and the atomic level surface roughness of the substrate (surface effect) [31]. In any real system, more than one of these factors are in operation, preventing conclusive understanding from MD simulations. To study the effect of lattice misfit without any interference from chemical and surface factors, we have designed a generic metallic system: the liquid Al/pinned solid Al substrate system, in which liquid Al represents the liquid, while the pinned Al substrate represents the substrate. This generic system has the following advantages over the specific systems:

- Allowing systematic investigation of systems with varying lattice misfit, i.e., many different substrates.
- Elimination of the influence of both availability and reliability of potentials used for simulations [30,31].
- Elimination of the effects of chemistry and surface condition of the substrate.
- Pinned substrate represents a variety of high temperature substrates, such as oxides, nitrides and borides practice (e.g., TiB_2 with T_l = 3498 K [36]).

Therefore, our simulation results from this generic simulation system are scientifically more rigorous and practically more representative of heterogeneous nucleation, compared with results obtained from specific systems.

This nucleation system consists of a generic liquid and a generic fcc substrate with a <111> surface orientation, being parallel to the z axis. We chose aluminum as the generic liquid because: (1) it is representative of many metals in terms of liquid structures [37]; and (2) the potential of Al has been widely tested [28,38,39]. The generic fcc substrate lattice is built using pinned aluminum atoms with a specified lattice parameter to pre-set the lattice misfit [28]. For simplicity, hereafter, we use the generic terms 'the liquid' and 'the substrate' in this paper.

The initial dimensions were $48[11\bar{2}] \times 30[\bar{1}10] \times 15[111]$ for the liquid and $48[11\bar{2}] \times 30[\bar{1}10] \times 6[111]$ for the substrate, with the total number of atoms in the system being 5040. Periodic boundary conditions were imposed in the $x([11\bar{2}])$- and $y([\bar{1}10])$-directions. A vacuum region was inserted with periodic boundary conditions in the z-direction, and the extent of the vacuum region was 60 Å. The initial configuration of the fcc materials has a lattice parameter a = 4.126 Å, which corresponds to the value for aluminum obtained at its calculated melting point. The substrate was assigned a varied lattice misfit with the solid aluminum. The lattice misfit, f, between the substrate and solid Al is defined as

$$f = (d_S - d_N)/d_S \times 100\% \quad (1)$$

where d_S and d_N are the atomic spacing of the solid metal and the substrate, respectively. In this paper we confine ourselves to the systems with negative lattice misfit ($-8\% \leq f \leq 0\%$), with the systems with positive misfit being studied elsewhere [35].

The EAM (embedded atom method) potential for aluminum, developed by Zope and Mishin to model interatomic interactions [38], was used in this work. The predicted melting temperature for pure Al is 870 ± 4 K with this potential [38]. During the simulation, the Al atoms above the substrate were allowed to move freely under the effect of the interatomic potential. The substrate atoms were excluded from the equations of motion, but the forces they exert on the adjacent atoms were included. All the MD simulations were performed using the DL_POLY_4.08 MD package [40]. The equations of motion were integrated by means of the Verlet algorithm with a time step of 0.001 ps and the Berendsen NVT ensemble was used for the temperature control. The liquid was prepared by heating the system to a temperature of 1400 K with steps of 50 K, each lasting 100,000 MD steps. The total energy of the simulation system was used to monitor whether the system is equilibrated, and we found that 100,000 MD steps (1 ns) are adequate to ensure equilibrium in all the systems concerned in this paper.

The nucleation temperature, T_n, for each specified nucleation system was determined using the variable step search method. The equilibrated configuration of the liquid at 1400 K was cooled to a desired temperature with a step of 50 K and at each temperature step the system was allowed to run for 1,000,000 MD time steps, which has been checked to be sufficient to reach equilibrium in the current studies. The initial nucleation temperature, T_1, was determined by monitoring variation in total energy and trajectory of the system during the equilibration. This means that exact nucleation occurred in the temperature interval between T_1 and T_1 + 50 K. A more accurate nucleation temperature, T_2, was determined by a finer search in this reduced temperature interval with a temperature step of 5 K. Finally, the nucleation temperature, T_n, was determined by an even finer search between T_2 and T_2 + 5 K with a temperature step of 1 K. This approach allows the nucleation temperature to be determined within an error of ±1 K.

The atomic ordering in the liquid adjacent to the liquid/substrate interface was quantified using the atomic density profile for ordering along the z direction and in-plane order parameter for ordering in the x-y plane. Atomic density profile, $\rho(z)$, is defined as [41]

$$\rho(z) = \frac{\langle N_z \rangle}{L_x L_y \Delta z} \tag{2}$$

where N_z is the number of atoms between $z - \Delta z/2$ and $z + \Delta z/2$ at time t, Δz is the width of the bin, a 10th of the layer spacing in this study. The angled brackets indicate a time-averaged quantity, and L_x and L_y are the x and y dimensions of the cell.

The in-plane order parameter, $S(z)$, is defined as [42]

$$S(z) = \frac{\left|\sum_{j \in \Delta z} exp\left(i\boldsymbol{K}\cdot\boldsymbol{r}_j\right)\right|^2}{N_z^2} \tag{3}$$

where the summation is over all atoms labelled j within a given bin of width, Δz, of one layer spacing and $\boldsymbol{K}$ is a reciprocal lattice vector and $\boldsymbol{r}_j$ is the position vector of the jth atom in the Cartesian space. We chose $\boldsymbol{K} = \frac{\pi}{a}\left[2\sqrt{2}, 2\sqrt{6}, \sqrt{3}\right]$ such that $\exp(i\boldsymbol{K}\cdot\boldsymbol{r}_j) = 1$ for any $\boldsymbol{r}_j$ in a perfect fcc lattice with a [111] surface orientation. When all the atoms are at their perfect fcc (111) sites, the $S(z)$ will be 1 and the order parameter reduces the further they are away from their ideal positions.

The atomic arrangement in the liquid adjacent to the interface during the simulation is characterized by the time-averaged atomic positions [43] and local bond-order analysis [44]. The time-averaged atomic positions in the individual layers of the liquid within 10 ps were taken from the trajectory of the simulation. With this approach, the solid atoms can be distinguished from the liquid atoms, where the solid atoms usually vibrate at their equilibrium positions and the liquid atoms can move more than one atomic spacing [43]. The local bond-order analysis is another approach widely used in atomistic simulations to

distinguish the solid atoms from the liquid atoms in the bulk liquid [45]. To perform the local bond-order analysis, the local bond-order parameters, $q_l(i)$, were calculated as [43]

$$q_l(i) = \left(\frac{4\pi}{2l+1} \sum_{m=-l}^{l} |q_{lm}(i)|^2 \right)^{\frac{1}{2}} \quad (4)$$

where the $(2l + 1)$ dimensional complex vector $q_{lm}(i)$ is the sum of spherical harmonics, $Y_{lm}(r_{ij})$, over all the nearest neighboring atoms of the atom i. Two neighboring atoms i and j can be recognized to be connected if the correlation function, $q_6(i) \cdot q_6(j)$, of the vector q_6 of neighboring atoms i and j exceeds a certain threshold, 0.1 in this study. To distinguish the solid atoms from the liquid atoms, a threshold on the number of connections that an atom has with its neighbors is set to 6.

2.2. Experimental Methods

To facilitate direct examinations of samples using advanced electron microscopy a pressurized melt filtration technique [46] was used to collect TiB_2 particles introduced into the alloy melts (Al-8Si and Al-5Mg-3Si-0.6Mn-0.6Fe alloys) through the addition of stoichiometric Al-2.2Ti-1B grain refiner. During the pressurized melt filtration process, argon was introduced to force the melt to flow through a porous filter attached to the bottom of the crucible. The TiB_2 particles were collected above the filter together with the residual melt. The solidified material immediately above the filter, which contained the locally concentrated TiB_2 particles, was used to prepare samples for TEM examination. A more detailed description of the melt filtration technique can be found elsewhere [46].

Thin foil specimens for transmission electron microscopy (TEM) were prepared from 3 mm diameter discs sliced from the filtered residue material. The discs were ground to a thickness of less than 60 μm before further thinning by Ar ion beam milling using a Gatan precision ion polishing system (PIPS, Gatan Inc., Leicester, UK) under a voltage of 1.0–5.0 kV and an incident beam angle of 3–5°. High resolution TEM analysis was conducted on a JEOL 2100 F microscope (JEOL Ltd., Tokyo, Japan) operated with an accelerating voltage of 200 kV. The twist angle was determined by the double tilting experiments.

3. Results

3.1. Heterogeneous Nucleation Process

For a system with a lattice misfit $f = -8\%$, the nucleation temperature (T_n) was found to be 760 K, and the total energy (E_t) as a function of elapsed time, t, is plotted in Figure 1. E_t is constant until the onset of nucleation (t_1), from which the total energy decreases sharply between t_1 and t_3 and remains constant after t_3 (t_3 marks the end of solidification). The system is in the stage of the prenucleation before $t = 0$ ps (t_1). As shown later, $t = t_2 = 50$ ps marks the finish of nucleation. Figure 1 demonstrates that heterogeneous nucleation at T_n is a spontaneous process without any energy barrier. This is in clear contrast to the CNT, in which heterogeneous nucleation only occurs when an energy barrier is overcome by structural fluctuation in the disordered liquid at the interface. Figure 2 shows the time-averaged atomic positions at the interface during the simulation for the system with $f = -8\%$ at $T_n = 760$ K, showing the evolution of atomic arrangement at the stage of prenucleation. The first layer (L1) has a nearly fully ordered structure that contains stacking faults (marked as 'C') surrounded by partial edge dislocations; and the second layer (L2) and the third layer (L3) have gradually reduced ordered regions. Detailed analysis revealed that: (1) there exists a 2D ordered structure within the first three atomic layers at the interface; (2) the degree of ordering in this 2D ordered structure is a function of temperature; and (3) the 2D ordered structure is dynamic. This means that, at a given temperature, the position and size of an ordered region may change with time but the total degree of ordering will remain constant.

Figure 3a presents a snapshot of the system with $f = -8\%$ at $t = 0$ ps and $T = T_n = 760$ K, showing a layered structure in the liquid adjacent to the interface. The quantified atomic

density profiles, $\rho(z)$, and in-plane order parameter, $S(z)$, are plotted in Figure 3b,c as a function of distance, z, from the interface. There are six atomic layers at the interface, but only the first two show notable in-plane atomic ordering. The detailed atomic arrangements are shown in Figure 3d–g for the first four layers (L1–L4). L1 has a largely ordered structure except for some small disordered regions, L2 and L3 have a mixed structure with ordered and disordered regions, and L4 is largely disordered. The ordered structure in L1 has different domains, with either a B or C stacking sequence if the surface layer of the substrate is assigned to be A in the ABCA stacking sequence for fcc structures. The ordered regions with C stacking sequence are stacking faults bounded by Shockley partial dislocations (solid lines in Figure 3d), which are formed at the prenucleation stage (see [28]). There is a 2D ordered structure in the liquid adjacent to the interface immediately before nucleation (at t_1), which is induced by the substrate surface and stabilized by a reduction of interfacial energy. This stable 2D ordered structure at T_n represents the maximum degree of ordering achievable by prenucleation and will act as a precursor for heterogeneous nucleation. This is similar to the prenucleation clusters (PNCs) discovered recently in aqueous solution [19].

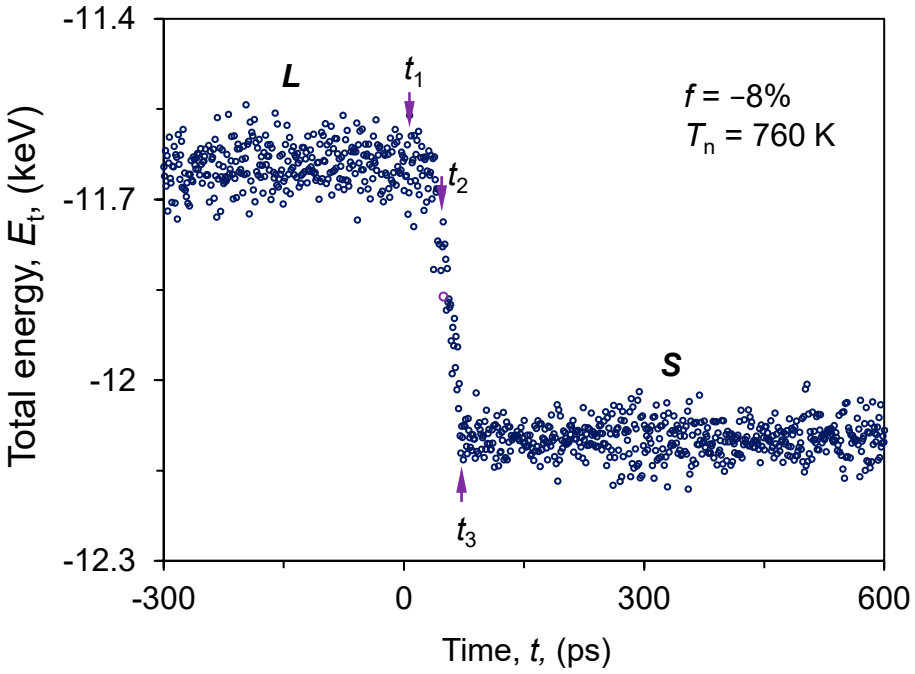

Figure 1. Evolution of total energy (E_t) of the system with $f = -8\%$ during the simulation at $T_n = 760$ K. $t = 0$ marks the onset of nucleation, t_1 marks the onset of nucleation, t_2 the end of nucleation and t_3 the end of solidification. L and S denote the liquid and the solid phases, respectively.

The evolution of atomic ordering at the interface during heterogeneous nucleation is shown in Figure 4a–d for the system with $f = -8\%$ at $T_n = 760$ K, where only the solid atoms are displayed after the local bond-order analysis. At $t = 0$ ps, L1 consists of largely solid atoms, with regularly distributed stacking faults bounded by partial edge dislocations (Figure 4a). As time elapses, whilst the solid regions in L1 increases slightly, some of the ordered regions in L2 start to merge and the solid region in L3 starts to expand (Figure 4b,c). Shockley partial dislocations can be identified between the neighboring solid regions with different stacking sequences in L2. At $t = 50$ ps, all the first three layers consist of solid atoms. L3 has an atomic arrangement that is identical to the fcc (111) plane of the bulk solid Al (Figure 4d).

Figure 4 also demonstrates structural templating as a mechanism for achieving atomic ordering during heterogeneous nucleation. The ordered regions in one atomic layer provides low energy positions where potential solid atoms in the next layer can be located. In Figure 4a–d, all the solid atoms in a given atomic layer are located just above the central

position between three solid atoms in the underneath layer. There are no solid atoms that locate on top of liquid atoms. We refer to this process as 'structural templating'.

Figure 5a shows the fraction of solid atoms, f_s, in L1–L9 as a function of time for the system with $f = -8\%$ at 760 K. Before $t = 0$ ps, f_s remains nearly constant for each layer, 0.75 for L1, 0.4 for L2, 0.1 for L3, and 0 for the liquid further away from the interface. After $t = 0$ ps, f_s in L1 increases slightly from 0.75 at $t = 0$ ps to 0.85 at $t = 50$ ps and beyond. At the same time, the f_s values for L2 and L3 gradually increase to nearly 1 at $t = 50$ ps. The values of f_s for the subsequent layers increase rapidly from 0 to nearly 1 after the formation of the first three layers of the solid.

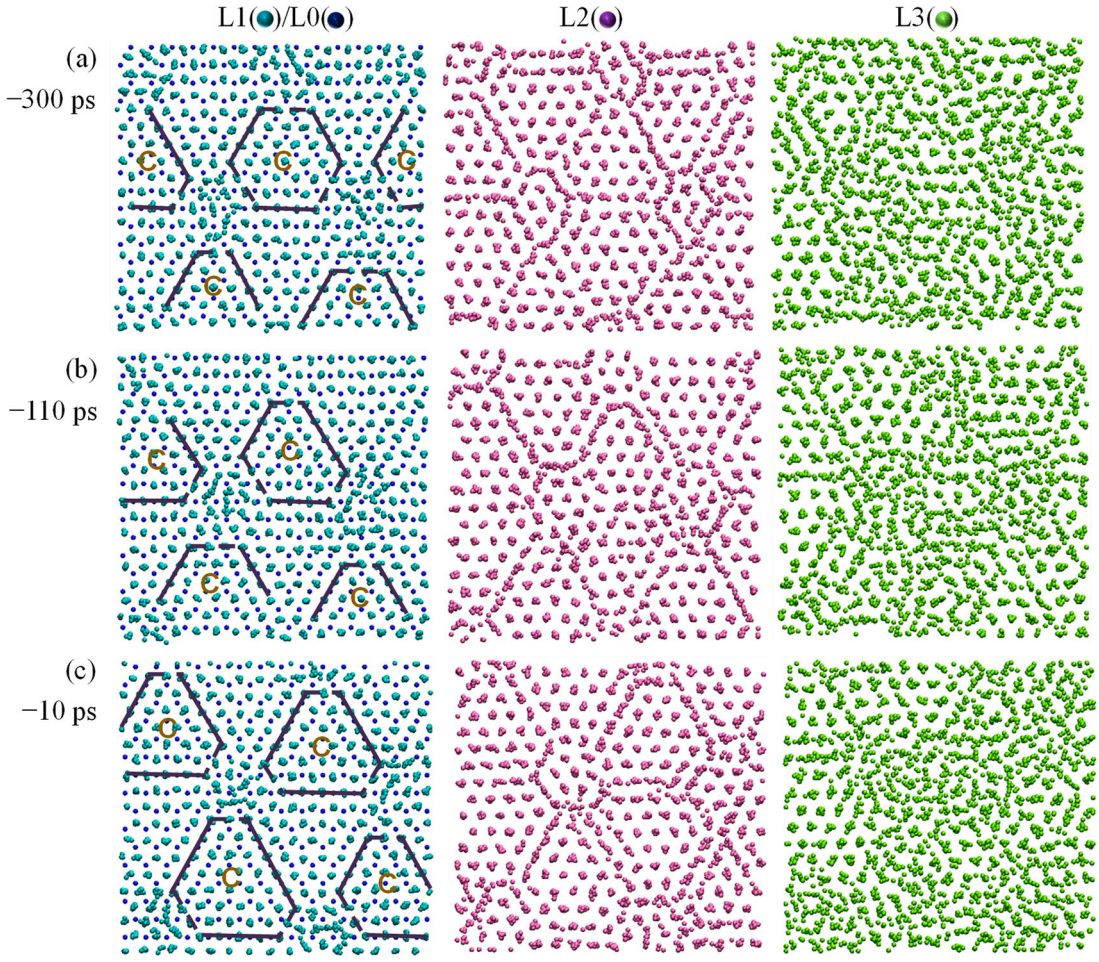

Figure 2. Evolution of the 2D ordered structure at the liquid/substrate interface in the system with $f = -8\%$ at $T_n = 760$ K. Time-averaged atomic positions of L1(on top of L0), L2 and L3 at (**a**) $t = -300$ ps; (**b**) $t = -110$ ps; and (**c**) $t = -10$ ps showing the dynamic nature of the 2D ordered structure. "C" marks the stacking fault that is surrounded by partial edge dislocations (the solid lines).

The densification process during the simulation was also quantified using the average spacing (d_a) of the solid atoms in the ordered regions in each layer, and Figure 5b shows d_a as a function of distance and time for the system with $f = -8\%$ at $T_n = 760$ K. The atomic spacings in L1 and L2 decrease gradually with time during the simulation, indicative of a densification process in the first two layers at the interface. In general, the spacing of solid atoms decreases with increasing distance from the interface and becomes constant from L3 onwards. This suggests that the lattice misfit is accommodated entirely by L1 and L2, with L3 being identical to the corresponding plane of the bulk solid.

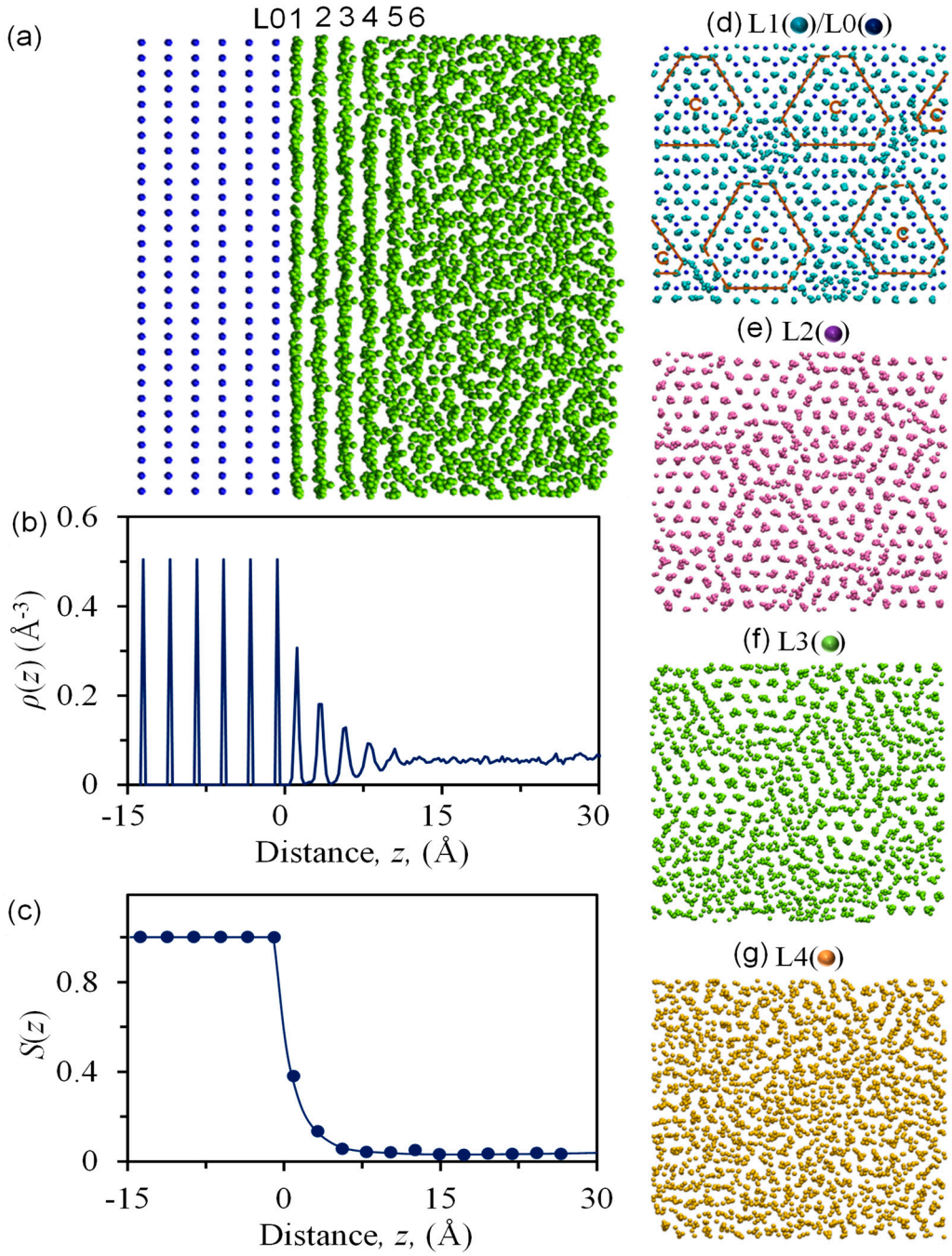

Figure 3. Precursor of heterogeneous nucleation. (**a**) A snapshot, and (**b**) atomic density profile, $\rho(z)$, and (**c**) in-plane order parameter, $S(z)$, as a function of the distance, z, from the interface at the onset of nucleation (t = 0 ps) for the simulation system with $f = -8\%$ at T_n = 760 K. There are six notable atomic layers in the liquid, but only the first two layers contain some degree of in-plane ordering. (**d**–**g**) Time-averaged atomic positions of the L1, L2, L3, and L4 layers at the interface are indicative of 2D ordered structure. For comparison, L0 is also shown in (**d**). "C" marks the stacking fault that is surrounded by partial edge dislocations (the solid lines).

The outcome of heterogeneous nucleation is a crystalline plane of the solid (L3 in Figure 4d), which provides a template for the epitaxial growth of the solid from the liquid. Figure 6a is a snapshot of the system with $f = -8\%$ at t = 50 ps and T_n = 760 K, showing nine atomic layers at the interface, compared to 6 layers at t = 0 ps (Figure 3a). Beyond L9, the atomic arrangement becomes disordered. The quantified density profile and in-plane order parameter are shown in Figure 6b,c as a function of distance from the interface. Beyond L3,

$S(z)$ decreases rapidly with distance from the liquid. $S(z)$ for L1 is lower than that for L2 and L3, due to the lattice distortion caused by the partial edge dislocation network in L1.

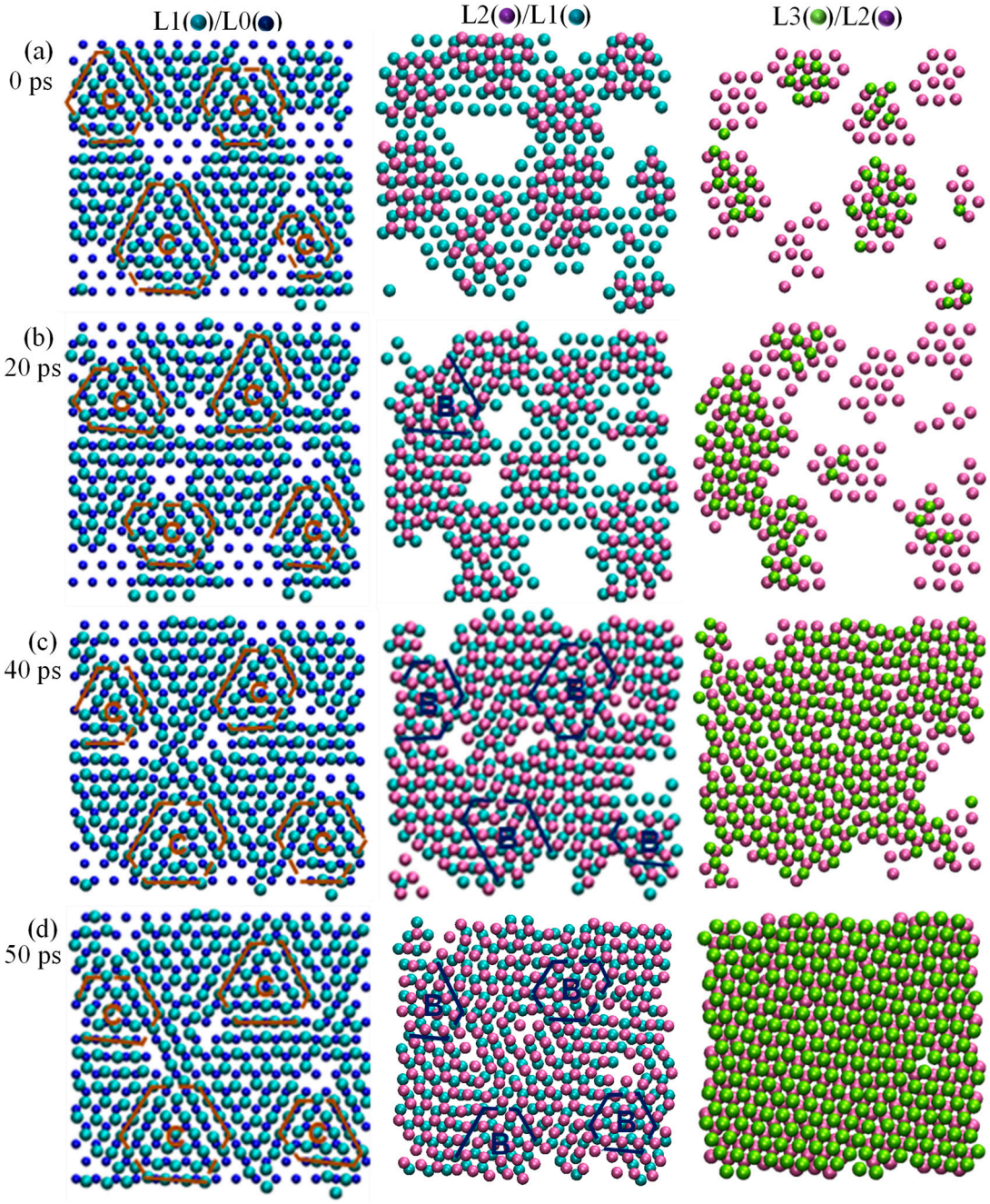

Figure 4. Evolution of atomic ordering through structural templating during nucleation. Atomic arrangements of the solid atoms at the interface as a function of time: (**a**) t = 0 ps, (**b**) 20 ps, (**c**) 40 ps, and (**d**) 50 ps during the simulation for the system with $f = -8\%$ at T_n = 760 K, where the liquid atoms have been removed from the snapshot. "C" and "B" mark the stacking fault that is surrounded by partial dislocations (the solid lines) in L1 and L2, respectively. Starting from the precursor created by prenucleation, nucleation proceeds layer-by-layer through structural templating: L1 accommodates lattice misfit via a partial edge dislocation network; L2 twists an angle of θ via a partial edge dislocation network to reduce lattice distortion; L3 is a nearly perfect plane of the solid that templates further growth.

Time-averaged atomic positions at the end of nucleation (t = 50 ps) are shown in Figure 6d–f. Using disregistry analysis [47], we identified the Shockley partial dislocations in L1 with Burgers vector (blue arrows) of $\boldsymbol{b}_1$, $\boldsymbol{b}_2$, and $\boldsymbol{b}_3$, which are largely normal to the

corresponding dislocation lines (orange lines), showing that the partial dislocations have a predominant edge component (Figure 6d). In L2, the Shockley partial dislocations with Burgers vector of $\boldsymbol{b}'_1$, $\boldsymbol{b}'_2$, and $\boldsymbol{b}'_3$ (orange arrows, Figure 6e) are largely parallel to the corresponding dislocation lines (blue lines), showing that they have a predominant screw component. The analysis shows that there are no dislocations in L3.

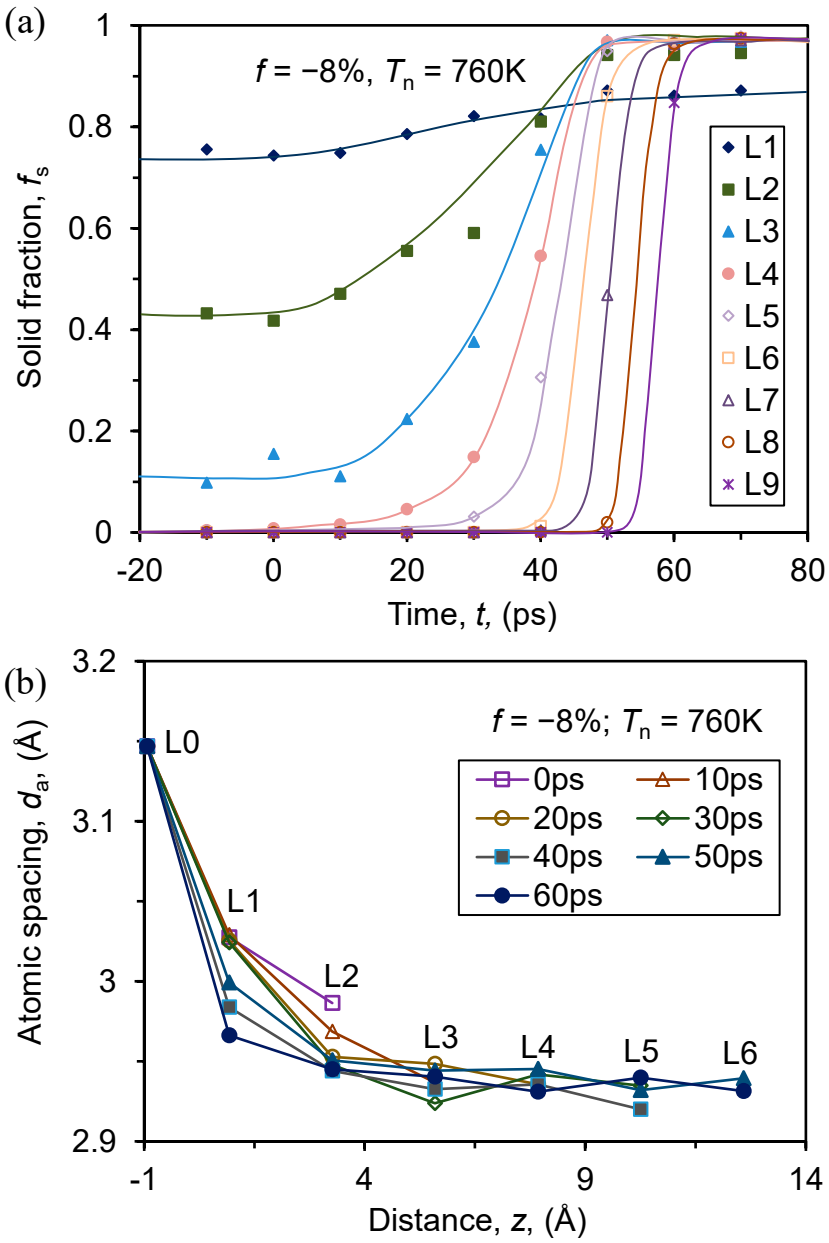

Figure 5. (**a**) Fraction of the solid atoms, f_s, and (**b**) average atomic spacing, d_a, of the ordered regions in the individual layer at the interface as a function of z and t during the simulation of the system with $f = -8\%$ at $T_n = 760$ K.

Heterogeneous nucleation of the crystal structure of a new phase occurs within the first three atomic layers. After the formation of L3, solidification enters the growth stage. The nucleation process is characterized by a gradual increase of atomic ordering through structural templating (Figure 5a) and a gradual decrease of atomic spacing (Figure 5b). In contrast, at the growth stage atomic ordering increases much faster (Figure 5a) through epitaxial growth without any change in atomic spacing (Figure 5b). There is only one interface (substrate/liquid) before nucleation (Figure 3), but two interfaces after nucleation

(a substrate/solid interface and a solid/liquid interface) (Figure 6), while growth is a process where the solid/liquid interface advances into the liquid.

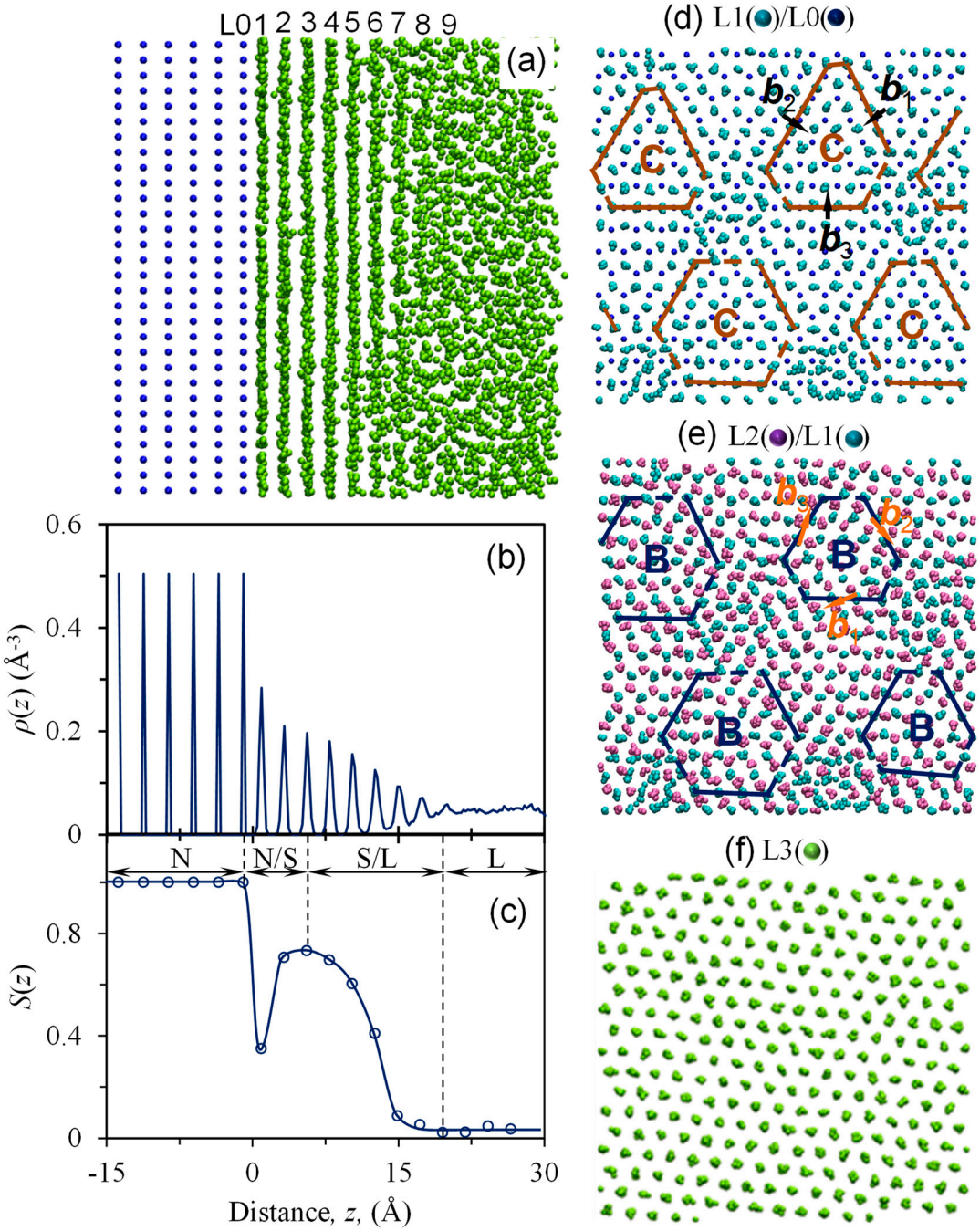

Figure 6. (**a**) A snapshot, and (**b**) $\rho(z)$, and (**c**) $S(z)$ as a function of z from the interface at t = 50 ps during the simulation for the system with $f = -8\%$ at T_n = 760 K. Time-averaged atomic positions of (**d**) L1 on top of L0 showing the partial edge dislocation network; (**e**) L2 on top of L1 showing the partial screw dislocation network; and (**f**) L3 showing a nearly perfect plane of the solid that templates further growth. The $\boldsymbol{b}_1$, $\boldsymbol{b}_2$, $\boldsymbol{b}_3$ ($\boldsymbol{b}'_1$, $\boldsymbol{b}'_2$, $\boldsymbol{b}'_3$) and the arrows represent the Burges vectors of the Shockley partial edge (screw) dislocations in the L1 (L2).

3.2. Effect of Lattice Misfit

The evolution of atomic ordering during the nucleation process is qualitatively similar for all systems with negative misfit. Figure 7 shows the time-averaged atomic positions of L1/L0, L2/L1, and L3 for the systems with $f = -2\%$, -6% and -8% at t = 1 ns (fully

solidified) in the simulations at their respective T_n (833 K, 764 K and 760 K for the systems with $f = -2\%$, -6%, and -8%). The density of the partial dislocations in L1 and L2 increases with misfit. L3 is a nearly perfect crystalline plane of the fcc Al lattice, regardless of the misfit. The three-layer atomistic mechanism for heterogeneous nucleation is consistent for systems with negative misfit regardless of the degree of misfit.

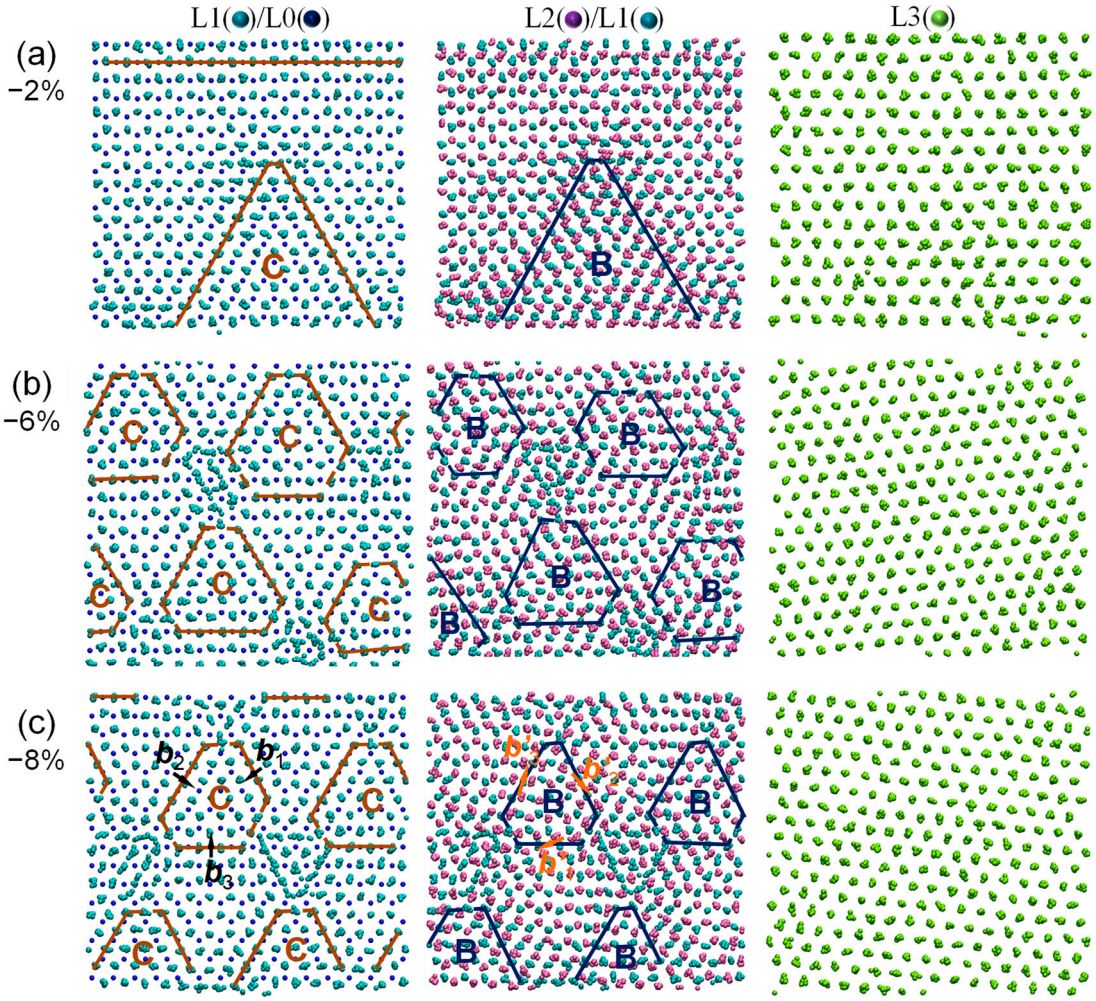

Figure 7. Time-averaged atomic positions at the interface for the systems with (**a**) $f = -2\%$, (**b**) -6%, and (**c**) -8% at $t = 1$ ns during the simulations at their respective T_n. The $\boldsymbol{b}_1$, $\boldsymbol{b}_2$, $\boldsymbol{b}_3$ ($\boldsymbol{b'}_1$, $\boldsymbol{b'}_2$, $\boldsymbol{b'}_3$) and the arrows represent the Burges vectors of the Shockley partial edge (screw) dislocations in the L1 (L2).

The edge component of the partial dislocations in L1 accommodates the initial misfit and, the accommodated misfit, f_a, in the individual layer at the interface can be obtained by calculating the ratio of the average atomic spacing of each layer relative to that of the substrate. For the system with an initial misfit of $f = -8\%$, L1 and L2 accommodates -6.7% and -1.3% misfit, respectively. Figure 8a shows f_a for L1 as a function of the initial misfit f. The absolute value of accommodated misfit ($|f_a|$) by L1 increases with increasing absolute value of misfit ($|f|$) of the system, and the value of f_a in L1 accounts for most of the initial f for all the systems studied.

One of the interesting phenomena revealed in this work is that, after nucleation, the solid twists an angle relative to the substrate (Figure 7). We evaluated the twist angle of the individual layer relative to the substrate as an average over the acute angles between three close-packed directions (<110>) of the consecutive layers at the interface. For the system with $f = -8\%$, the calculated twist angle, θ, is 4.8° for L2 relative to L1, and 1.2° for L1 relative to the substrate surface, making a total twist angle of 6.0°. The twist is achieved

through the screw component of partial dislocations in L2 and L1. Figure 8b shows the total twist angle, θ, of the solid relative to the substrate as a function of the initial misfit, f. The twist angle of the solid increases with increasing initial misfit, from 0° for f = 0% to about 6° for $f = -8\%$.

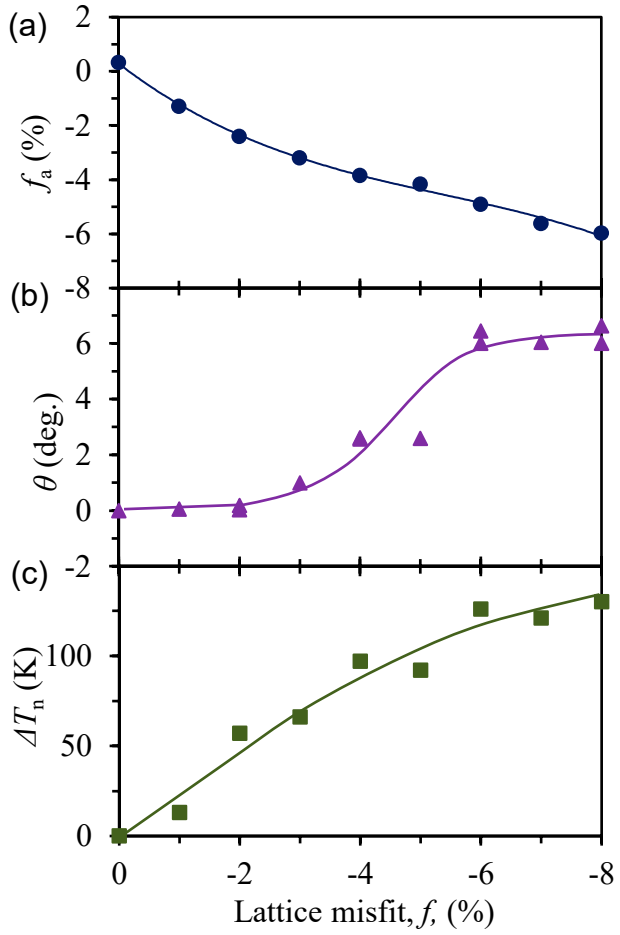

Figure 8. (**a**) Accommodated lattice misfit, f_a, in L1, (**b**) the twisted angle, θ, of the solid relative to the substrate, and (**c**) nucleation undercooling, ΔT_n, as a function of the initial lattice misfit, f.

The nucleation undercooling, ΔT_n, is the difference between the liquidus (T_l) and the nucleation temperature (T_n): $\Delta T_n = T_l - T_n$. In this work, we take ΔT_n = 0 K for the system with f = 0% as the reference point and then ΔT_n for systems with varying f can be determined. The calculated ΔT_n as a function of misfit is plotted in Figure 8c, which shows that nucleation undercooling increases with increasing misfit ($0 \leq |f| \leq -8\%$).

3.3. A New Atomistic Mechanism for Heterogeneous Nucleation

Based on the above results, here we present a new atomistic mechanism for heterogeneous nucleation, which is schematically illustrated in Figure 9, and can be described as follows:

- Prenucleation creating a 2D ordered structure that acts as a precursor for nucleation.
- Accommodation of misfit by forming a partial edge dislocation network in L1.
- Relaxation of the lattice distortion by twisting L2 by an angle (θ) through the formation of a partial screw dislocation network in L2.
- Completion of nucleation by creating a crystal plane of the solid (L3) that provides a template for further growth.

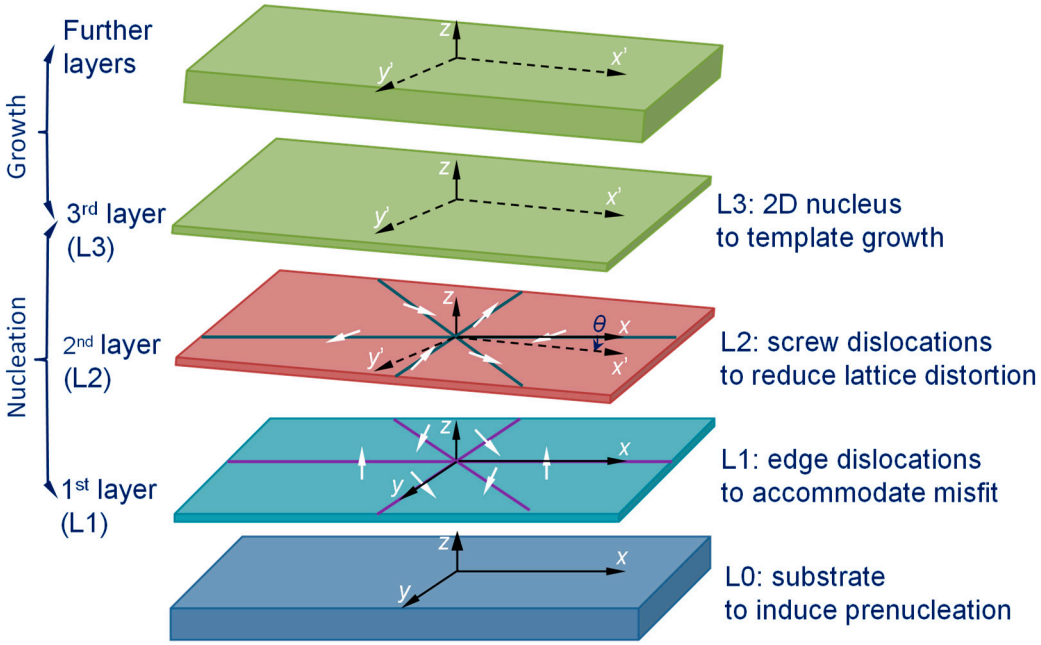

Figure 9. Schematic illustration of the three-layer nucleation mechanism for the system with negative lattice misfit. Building on the precursor (a 2D ordered structure) induced by the substrate at the prenucleation stage, at nucleation temperature, heterogeneous nucleation proceeds layer-by-layer through structural templating. L1 accommodates lattice misfit through an edge dislocation network; L2 twists an angle to reduce lattice distortion; and L3 is a plane of the solid (the 2-D nucleus) that templates further growth.

3.4. Experimental Validation

Heterogeneous nucleation in metallic liquids takes place at liquid/substrate interface buried deeply in an opaque liquid at high temperature, in an extremely short time interval and at nanometer length scale. This makes *in situ* experimental observation of heterogeneous nucleation process extremely difficult, if at all possible. However, postmortem approach may be used to examine some of the useful signatures of heterogeneous nucleation. As shown in Figures 8 and 9, one of the key features of the three-layer nucleation mechanism for systems with negative lattice misfit is that upon completion of nucleation the new solid phase twists an angle (θ) relative to the substrate and that the twist angle increases with increasing lattice misfit. This phenomenon provides us with an approach to validate, at least partially, the three-layer nucleation mechanism based on MD simulations.

In this work, we have undertaken experimental work to confirm the twist angle related to the lattice misfit. TiB_2 particles with a (0001) surface termination (denoted as (0001) TiB_2) have a misfit of −4.2% with the (111) Al at 660 °C according to the following orientation relationship (OR) [16]

$$(0001)\left[11\bar{2}0\right]\ TiB_2\ //\ (111)\left[0\bar{1}1\right]\ Al \qquad \text{(OR1)}$$

Figure 10a is a HRTEM micrograph showing the interface between (0001) TiB_2 and (111) Al, where the electron beam is parallel to the $\left[11\bar{2}0\right]$ TiB_2 direction. The first layer of aluminum atoms on the (0001) TiB_2 surface has an epitaxial relationship with the substrate (shown as individual lattice with edge dislocations), whilst from the 2nd layer onwards, the aluminum lattice has twisted by an angle of 4.7° along the [1] TiB_2 axis as measured by double tilting experiments and confirmed by the striation of the rest of (111) aluminum planes. Another example is found in the solidified Al-5Mg-3Si-0.6Mn-0.6Fe alloy with TiB_2 addition. Figure 10b is a HRTEM micrograph showing the atomic arrangement across the

TiB_2/α-$Al_{15}(Fe, Mn)_3Si_2$ interface, where the electron beam is parallel to the $[01\bar{1}]$ direction of the α-$Al_{15}(Fe, Mn)_3Si_2$ crystal. The OR between TiB_2 and α-$Al_{15}(Fe, Mn)_3Si_2$ is

$$(0001)[11\bar{2}0]\ TiB_2\ //\ (01\bar{1})[111]\ \alpha - Al_{15}(Fe,\ Mn)_3Si_2 \quad \text{(OR2)}$$

The lattice misfit determined by OR2 is −5.5%. We found that α-$Al_{15}(Fe, Mn)_3Si_2$ has twisted 4.5° along the [1] TiB_2 axis. These results presented in Figure 10a,b provide directly support to the nucleation mechanism illustrated in Figure 9.

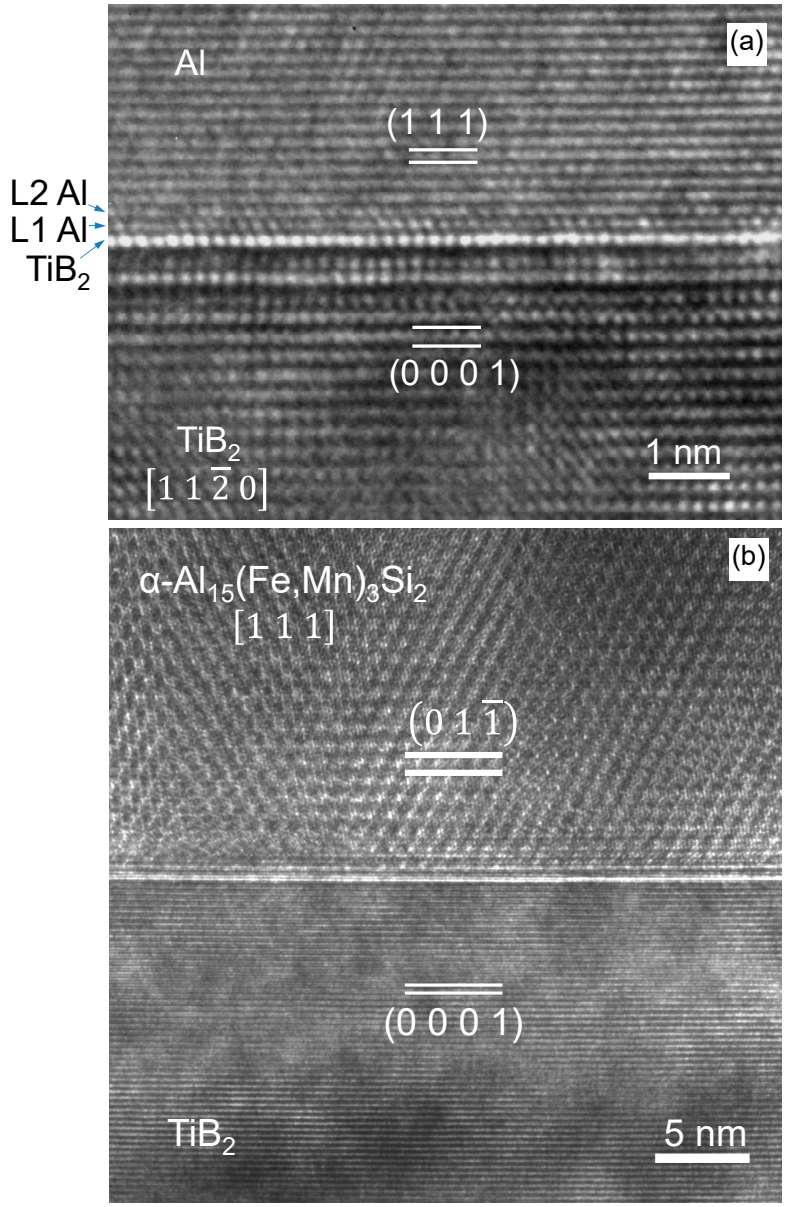

Figure 10. High resolution TEM micrographs show that, on the (0001) TiB_2 substrate, there exists an epitaxial first layer and a twist of the nucleated crystals relative to the substrate. (**a**) α-Al phase and (**b**) α-$Al_{15}(Fe, Mn)_3Si_2$ phase nucleated on the (0001) TiB_2 substrate showing a 4.7° and 4.5° twist relative to the TiB_2 substrate, respectively. The observed twist angles are in good agreement with the results from MD simulations (Figure 8b), providing an experimental support to the proposed nucleation mechanism (Figure 9).

In addition, a three-layer nucleation mechanism was established in the systems with positive lattice misfit by MD simulations [35], where the first layer is epitaxial to the

substrate surface, the second layer contains vacancies to accommodate lattice misfit, and the third layer becomes a plane of the solid (i.e., the 2D nucleus), involving no twist of the solid relative to the substrate. This no-twist signature of heterogenous nucleation in the systems with positive lattice misfit is supported by an earlier HRTEM examination. Fan et al. [46] investigated the grain refinement mechanisms in AZ91D Mg-alloy, and found that MgO particles can nucleate α-Mg with the following OR

$$< 01\bar{1} > \{111\}\ \mathrm{MgO}\ //\ < 1\bar{2}10 > \{0002\}\ \mathrm{Mg} \quad \text{(OR3)}$$

which gives a lattice misfit of 7.9%. There is no twist observed between the two crystals, being in good agreement with the MD simulation.

4. Discussion

By using MD simulations, we have established an atomistic mechanism for heterogeneous nucleation process for systems with negative misfit, as schematically illustrated in Figure 9. The substrate surface induces a 2D ordered structure in the liquid adjacent to the interface at temperatures above T_n, and this is termed prenucleation [28]. Our previous work found that prenucleation is affected by temperature [28,30], lattice misfit [28], chemical interaction between the substrate and the liquid [26] and the atomic-level surface roughness of the substrate [31]. For a given nucleation system the degree of prenucleation increases with decreasing temperature and reaches a maximum level at T_n (Figure 3). Prenucleation creates a precursor for heterogeneous nucleation. At T_n, building on the precursor, heterogeneous nucleation starts by completing the atomic ordering of L1 where the initial misfit in the system has been largely accommodated by the formation of a partial edge dislocation network (Figure 4). A consequence of the partial dislocation network is the distortion of the atomic lattice in L1, where the atomic rows become zig-zagged (Figure 4). This increase in atomic ordering in L1 templates more atomic ordering in L2, which twists by an angle (θ) to reduce the lattice distortion through the formation of a network of partial screw dislocations (Figure 6e). A crystalline plane of the solid is created in L3 (Figure 6f), and L3 becomes the template (i.e., 2D nucleus) for epitaxial growth of the new solid phase.

Based on the above description, heterogeneous nucleation can be defined as a process that creates a crystal plane of the solid (2D nucleus) from which the solid can grow. This is in clear contrast to the cap formation (3D nucleus) in the classical nucleation theory (CNT). This concept of heterogeneous nucleation makes a number of advances over the CNT:

- The liquid phase: The CNT assumes that the liquid is a disordered phase containing instantaneous short-range order (unstable). In contrast, the new concept acknowledges the importance of prenucleation that provides a stable 2D ordered structure as a precursor for heterogeneous nucleation (Figure 3).
- The interface: The CNT assumes that all the interfaces are sharp with zero thickness (the capillarity assumption), while the new concept suggests that all the interfaces are diffuse with finite thickness (Figure 6). Such diffuse interface can be quantified by atomic density profile ($\rho(z)$) and in-plane order parameter ($S(z)$).
- Nucleation outcome: The outcome of classical heterogeneous nucleation is a spherical cap of the solid with a critical radius (3D), while in the new concept heterogeneous nucleation provides a crystalline plane of the solid (2D).
- Energy barrier: In the CNT, there may be an energy barrier for heterogeneous nucleation depending on the nucleation undercooling (ΔT_n), while in the new concept heterogeneous nucleation is a down-hill process with no energy barrier.
- Atomic ordering mechanism: the CNT relies on structural fluctuation to provide the critical nucleus and thus is a stochastic process, while in the new concept nucleation starts from the precursor provided by prenucleation, proceeds layer-by-layer through structural templating (Figure 9), and therefore is a deterministic process.

Based on the capillarity assumption the CNT is mathematically rigorous and self-consistent but represents a closed theoretical system that is difficult to make any tangible improvement on it. In contrast, the new concept of heterogeneous nucleation is an open framework to which new knowledge can be added. For instance, nucleation potency measured by nucleation undercooling is related to misfit, chemical interaction across the interface and atomic level surface roughness of the substrate. Such understanding provides approaches to manipulating the atomic arrangement at the substrate/liquid interface to either enhance or impede heterogeneous nucleation.

This study reveals that the potency of the substrate is primarily related to the lattice misfit (Figure 8c), in accordance with the prediction of the analytical models [48,49]. Here we take TiB_2 particles in Al melt as an example to demonstrate how a substrate can be manipulated to change nucleation potency. TiB_2 has a hexagonal crystal structure and a hexagonal platelet morphology with the (0001) planes as its major surface termination. The (0001) TiB_2 surface has a misfit of −4.2% with {111} Al at 660 °C [16], suggesting that TiB_2 is not potent for heterogeneous nucleation of aluminum. Segregation of Ti at the TiB_2/liquid Al interface leads to the formation of a mono atomic layer of (112) Al_3Ti 2DC, which reduces the misfit $|f|$ from 4.2% to 0.09%, significantly increasing the nucleation potency of TiB_2 particles [16]. However, addition of 500 ppm Zr into liquid Al results in the formation of (0001) Ti_2Zr 2DC on (0001) TiB_2 surface to replace the original (112) Al_3Ti 2DC [50]. The (0001) Ti_2Zr 2DC has not only a large misfit with Al but also an atomically rough surface, making such TiB_2 particles impotent for heterogenous nucleation of solid Al.

In addition to earlier work on the systems with positive lattice misfit [35], this work has extended the applicability of the three-layer nucleation mechanism to systems with negative misfit. This means that the three-layer nucleation mechanism is applicable to systems with small lattice misfit, i.e., $|f| < 12.5\%$, the theoretical upper limit of misfit for dislocation mechanisms [48]. However, further work is required to investigate the nucleation mechanisms for systems with large lattice misfit (i.e., $|f| > 12.5\%$) and/or with atomic-level surface roughness.

5. Summary

We have investigated systematically the heterogeneous nucleation mechanism in generic systems with negative misfits using molecular dynamics simulations. We found that heterogeneous nucleation starts from a 2D ordered structure created by prenucleation and finishes within three atomic layers to create a crystal plane of the solid that acts as a template for further growth. During the nucleation process, the first layer accommodates misfit through the formation of a partial edge dislocation network; the second layer reduces the lattice distortion in the first layer by twisting by an angle of θ through the formation of a partial screw dislocation network; and the third layer finishes nucleation and provides a template for growth. In addition, we found that the nucleation undercooling increase with increasing misfit, in agreement qualitatively with the previous theoretical predictions. The new concept of heterogeneous nucleation provides a number of advances compared with the classical nucleation theory (CNT); heterogeneous nucleation is a deterministic process that proceeds spontaneously (without an energy barrier) through a structural templating process. Furthermore, the MD simulation has confirmed that the heterogeneous nucleation in systems with negative lattice misfit results in a twist of the solid relative to the substrate, and that the twist angle increases with the lattice misfit. The twist angle as a signature of heterogeneous nucleation has been validated in Al-alloys using advanced electron microscopy.

Author Contributions: Z.F. conducted conceptualization of the research, development of the research approach, funding acquisition, supervision and original draft writing; H.M. conducted MD simulations and visualization; Y.W. and Z.Q. conducted experimental validation; and all the authors contributed to review and editing of the manuscript. All authors have read and agreed to the published version of the manuscript.

Funding: This work has been funded by the EPSRC of the UKRI under the grant number EP/N007638/1.

Data Availability Statement: All data is available in the main text.

Conflicts of Interest: The authors declare no conflict of interest.

References

1. Kelton, K.F.; Greer, A.L. Introduction. In *Nucleation in Condensed Mater: Applications in Materials and Biology*; Pergamon, Elsevier: Oxford, UK, 2010.
2. Kashchiev, D. *Nucleation: Basic Theory with Applications*; Butterworth-Heinemann: Oxford, UK, 2000.
3. Bartels-Rausch, T. Chemistry: Ten things we need to know about ice and snow. *Nature* **2013**, *494*, 27–29. [CrossRef]
4. Sosso, G.C.; Chen, J.; Cox, S.J.; Fitzner, M.; Pedevilla, P.; Zen, A.; Michaelides, A. Crystal nucleation in liquids: Open questions and future challenges in molecular dynamics simulations. *Chem. Rev.* **2016**, *116*, 7078–7116. [CrossRef]
5. Greer, A.L. Overview: Application of heterogeneous nucleation in grain-refining of metals. *J. Chem. Phys.* **2016**, *145*, 211704. [CrossRef]
6. Erdemir, D.; Lee, A.Y.; Myerson, A.S. Polymorph selection: The role of nucleation, crystal growth and molecular modeling. *Curr. Opin. Drug Discov. Dev.* **2007**, *10*, 746–755.
7. Michaels, T.C.T.; Šarić, A.; Curk, S.; Bernfur, K.; Arosio, P.; Meisl, G.; Dear, A.J.; Cohen, S.I.A.; Dobson, C.M.; Vendruscolo, M.; et al. Dynamics of oligomer populations formed during the aggregation of Alzheimer's Aβ42 peptide. *Nat. Chem.* **2020**, *12*, 445–451. [CrossRef]
8. Easton, M.; Qian, M.; Prasad, A.; StJohn, D. Recent advances in grain refinement of light metals and alloys. *Curr. Opin. Solid State Mater. Sci.* **2016**, *20*, 13–24. [CrossRef]
9. Gibbs, J.W. On the equilibrium of heterogeneous substances. *Am. J. Sci.* **1878**, *s3-16*, 441–458. [CrossRef]
10. Volmer, M.; Weber, A.Z. Nucleus formation in supersaturated systems. *Zeitschrift für Physikalische Chemie* **1926**, *119*, 277–301.
11. Becker, R.; Döring, W. Kinetic treatment of nucleation in supersaturated vapors. *Ann. Phys. (Leipzig)* **1935**, *416*, 719–752. [CrossRef]
12. Zeldovich, Y.B. On the theory of new phase formation. Cavitation. *Acta Physicochem* **1943**, *18*, 1–22.
13. Cantor, B. Heterogeneous nucleation and adsorption. *Philos. Trans. R. Soc. A Math. Phys. Eng. Sci.* **2003**, *361*, 409–417. [CrossRef]
14. Russo, J.; Tanaka, H. Crystal nucleation as the ordering of multiple order parameters. *J. Chem. Phys.* **2016**, *145*, 211801. [CrossRef]
15. Lutsko, J.F. Novel paradigms in nonclassical nucleation theory. In *New Perspectives on Mineral Nucleation and Growth: From Solution Precursors to Solid Materials*; Van Diessche, A.E.S., Kellermeier, M., Benning, L.G., Gebauer, D., Eds.; Springer International Publishing: Cham, Switzerland, 2017.
16. Fan, Z.; Wang, Y.; Zhang, Y.; Qin, T.; Zhou, X.R.; Thompson, G.E.; Pennycook, T.; Hashimoto, T. Grain refining mechanism in the Al/Al-Ti-B system. *Acta Mater.* **2015**, *84*, 292–304. [CrossRef]
17. Zhou, J.; Yang, Y.; Yang, Y.; Kim, D.S.; Yuan, A.; Tian, X.; Ophus, C.; Sun, F.; Schmid, A.K.; Nathanson, M.; et al. Observing crystal nucleation in four dimensions using atomic electron tomography. *Nat. Cell Biol.* **2019**, *570*, 500–503. [CrossRef]
18. Shibuta, Y.; Sakane, S.; Miyoshi, E.; Okita, S.; Takaki, T.; Ohno, M. Heterogeneity in homogeneous nucleation from billion-atom molecular dynamics simulation of solidification of pure metal. *Nat. Commun.* **2017**, *8*, 1–9. [CrossRef]
19. Gebauer, D.; Völkel, A.; Cölfen, H. Stable prenucleation calcium carbonate clusters. *Science* **2008**, *322*, 1819–1822. [CrossRef] [PubMed]
20. Vekilov, P.G. The two-step mechanism of nucleation of crystals in solution. *Nanoscale* **2010**, *2*, 2346–2357. [CrossRef] [PubMed]
21. Chen, J.; Zhu, E.; Liu, J.; Zhang, S.; Lin, Z.; Duan, X.; Heinz, H.; Huang, Y.; De Yoreo, J.J. Building two-dimensional materials one row at a time: Avoiding the nucleation barrier. *Science* **2018**, *362*, 1135–1139. [CrossRef] [PubMed]
22. Kaplan, W.D.; Kauffmann, Y. Structural order in liquids induced by interfaces with crystals. *Annu. Rev. Mater. Res.* **2006**, *36*, 1–48. [CrossRef]
23. Oh, S.H.; Kauffmann, Y.; Scheu, C.; Kaplan, W.D.; Rühle, M. Ordered liquid aluminium at the interface with sapphire. *Science* **2005**, *310*, 661–663. [CrossRef] [PubMed]
24. Kauffmann, Y.; Oh, S.H.; Koch, C.T.; Hashibon, A.; Scheu, C.; Rühle, M.; Kaplan, W.D. Quantitative analysis of layering and in-plane ordering at an alumina-aluminium solid-liquid interface. *Acta Mater.* **2011**, *59*, 4378–4386. [CrossRef]
25. Geysermans, P.; Gorse, D.; Pontikis, V. Molecular dynamics study of the solid–liquid interface. *J. Chem. Phys.* **2000**, *113*, 6382–6389. [CrossRef]
26. Hashibon, A.; Adler, J.; Finnis, M.W.; Kaplan, W.D. Atomistic study of structural correlations at a liquid–solid interface. *Comput. Mater. Sci.* **2002**, *24*, 443–452. [CrossRef]
27. Yang, Y.; Olmsted, D.L.; Asta, M.; Laird, B.B. Atomistic characterization of the chemically heterogeneous Al–Pb solid–liquid interface. *Acta Mater.* **2012**, *60*, 4960–4971. [CrossRef]
28. Men, H.; Fan, Z. Prenucleation induced by crystalline substrates. *Metall. Mater. Trans. A* **2018**, *49*, 2766–2777. [CrossRef]
29. Palafox-Hernandez, J.P.; Laird, B.B.; Asta, M. Atomistic characterization of the Cu-Pb solid-liquid interface. *Acta Mater.* **2011**, *59*, 3137–3144. [CrossRef]
30. Fang, C.M.; Men, H.; Fan, Z. Effect of substrate chemistry on prenucleation. *Met. Mater. Trans. A* **2018**, *49*, 6231–6242. [CrossRef]
31. Jiang, B.; Men, H.; Fan, Z. Atomic ordering in the liquid adjacent to an atomically rough solid surface. *Comput. Mater. Sci.* **2018**, *153*, 73–81. [CrossRef]

32. Wang, L.; Lu, W.; Hu, Q.; Xia, M.; Wang, Y.; Li, J.-G. Interfacial tuning for the nucleation of liquid AlCu alloy. *Acta Mater.* **2017**, *139*, 75–85. [CrossRef]
33. Schülli, T.U.; Daudin, R.; Renaud, G.; Vaysset, A.; Geaymond, O.; Pasturel, A. Substrate-enhanced supercooling in AuSi eutectic droplets. *Nature* **2010**, *464*, 1174–1177. [CrossRef] [PubMed]
34. Wang, J.; Horsfield, A.; Schwingenschlögl, U.; Lee, P.D. Heterogeneous nucleation of solid Al from the melt by TiB_2 and Al_3Ti: An *ab initio* molecular dynamics study. *Phys. Rev. B* **2010**, *82*, 184203. [CrossRef]
35. Fan, Z.; Men, H. A molecular dynamics study of heterogeneous nucleation in generic liquid/substrate systems with positive lattice misfit. *Mater. Res. Express* **2020**, *7*, 126501. [CrossRef]
36. Munro, R.G. Material properties of titanium diboride. *J. Res. Natl. Inst. Stand. Technol.* **2000**, *105*, 709–720. [CrossRef] [PubMed]
37. Structure. Iida, T.; Guthrie, R.I.L. (Eds.) In *The Physical Properties of Liquid Metals*; Clarendon Press: Oxford, UK; Oxford University Press: New York, NY, USA, 1988.
38. Zope, R.R.; Mishin, Y. Interatomic potentials for atomistic simulations of the Ti-Al system. *Phys. Rev. B* **2003**, *68*, 024102. [CrossRef]
39. Wang, J.S.; Horsfield, A.; Lee, P.D.; Brommer, P. Heterogeneous nucleation of solid Al from the melt by Al_3Ti: Molecular dynamics simulations. *Phys. Rev. B* **2010**, *82*, 144203. [CrossRef]
40. Todorov, I.T.; Smith, W.; Trachenko, K.; Dove, M.T. DL_POLY_3: New dimensions in molecular dynamics simulations via massive parallelism. *J. Mater. Chem.* **2006**, *16*, 1911–1918. [CrossRef]
41. Hashibon, A.; Adler, J.; Finnis, M.W.; Kaplan, W.D. Ordering at solid-liquid interfaces between dissimilar materials. *Interface Sci.* **2001**, *9*, 175–181. [CrossRef]
42. Hook, J.R.; Hall, H.E. Scattering of neutrons and electrons from solids. In *Solid State Physics*, 2nd ed.; Wiley: Chichester, UK, 1991.
43. Jackson, K.A. The interface kinetics of crystal growth processes. *Interface Sci.* **2002**, *10*, 159–169. [CrossRef]
44. Steinhardt, P.J.; Nelson, D.R.; Ronchetti, M. Bond-orientational order in liquids and glasses. *Phys. Rev. B* **1983**, *28*, 784–805. [CrossRef]
45. Baumgartner, J.; Dey, A.A.; Bomans, P.H.H.; Le Coadou, C.; Fratzl, P.; Sommerdijk, N.A.J.M.; Faivre, D. Nucleation and growth of magnetite from solution. *Nat. Mater.* **2013**, *12*, 310–314. [CrossRef]
46. Fan, Z.; Wang, Y.; Xia, M.; Arumuganathar, S. Enhanced heterogeneous nucleation in AZ91D alloy by intensive melt shearing. *Acta Mater.* **2009**, *57*, 4891–4901. [CrossRef]
47. Hirth, J.; Pond, R.; Hoagland, R.; Liu, X.-Y.; Wang, J. Interface defects, reference spaces and the Frank–Bilby equation. *Prog. Mater. Sci.* **2013**, *58*, 749–823. [CrossRef]
48. Fan, Z. An epitaxial model for heterogeneous nucleation on potent substrates. *Met. Mater. Trans. A* **2012**, *44*, 1409–1418. [CrossRef]
49. Turnbull, D.; Vonnegut, B. Nucleation catalysis. *Ind. Eng. Chem.* **1952**, *44*, 1292–1298. [CrossRef]
50. Wang, Y.; Fang, C.; Zhou, L.; Hashimoto, T.; Zhou, X.; Ramasse, Q.; Fan, Z. Mechanism for Zr poisoning of Al-Ti-B based grain refiners. *Acta Mater.* **2019**, *164*, 428–439. [CrossRef]